

# Simple Rules Determine Distinct Patterns of Branching Morphogenesis

Wei Yu,<sup>1,2,8</sup> Wallace F. Marshall,<sup>3,4,8</sup> Ross J. Metzger,<sup>1,5</sup> Paul R. Brakeman,<sup>6</sup> Leonardo Morsut,<sup>2,7</sup> Wendell Lim,<sup>2,3</sup> and Keith E. Mostov<sup>1,3,4,\*</sup>

<sup>1</sup>Departments of Anatomy, University of California San Francisco, San Francisco, CA, USA

<sup>2</sup>Cell and Molecular Pharmacology, University of California San Francisco, San Francisco, CA, USA

<sup>3</sup>Center for Cellular Construction, University of California San Francisco, San Francisco, CA, USA

<sup>4</sup>Department of Biochemistry and Biophysics, University of California San Francisco, San Francisco, CA, USA

<sup>5</sup>Department of Pediatrics (Cardiology), Stanford University School of Medicine, Stanford, CA, USA

<sup>6</sup>Department of Pediatrics (Nephrology), University of California San Francisco, San Francisco, CA, USA

<sup>7</sup>Present address: Eli and Edyth Broad CIRM Center for Regenerative Medicine and Stem Cell Research, University of Southern California, Los Angeles, CA, USA

<sup>8</sup>These authors contributed equally

\*Correspondence: [keith.mostov@ucsf.edu](mailto:keith.mostov@ucsf.edu)

<https://doi.org/10.1016/j.cels.2019.08.001>

Many metazoan organs are comprised of branching trees of epithelial tubes; how patterning occurs in these trees is a fundamental problem of development. Commonly, branch tips fill the volume of the organ approximately uniformly, e.g., in mammalian lung, airway branch tips are dispersed roughly uniformly throughout the volume of the lung. In contrast, in the developing metanephric kidney, the tips of the ureteric bud tree are located close to the outer surface of the kidney rather than filling the kidney. Here, we describe a simple alteration in the branching rules that accounts for the difference between the kidney pattern that leads to tips near the organ surface versus previously known patterns that lead to the branch tips being dispersed throughout the organ. We further use a simple toy model to deduce from first principles how this rule change accounts for the differences in the two types of trees.

An age-old question in biology is how an organ develops into a particular form that reflects the function of the organ (Aristotle, 1961). For example, in metazoans, most internal organs consist of a tube lined by a layer of epithelial cells. In some cases, such as the vertebrate small intestine, this tube is unbranched. Partially digested food passes unidirectionally through the length of the intestinal tube while nutrients are absorbed by the lining epithelial cells (Walton et al., 2016). In other cases, the tube branches and forms a branching tree. Branching is a foundational process of developmental biology that leads from the cellular to the organ scale (Metzger and Krasnow, 1999).

Branching patterns can be divided into at least two broad classes. In many organs composed of a tree of branching tubes, the termini of the branches fill the volume of the organ approximately uniformly. For instance, in the mammalian lung, the branches of the respiratory tree are dispersed throughout the volume of the lung (Metzger et al., 2008), as shown in Figure 1A. Many exocrine glands—such as mammary, salivary, and pros-

tate—follow a similar pattern (Hannezo et al., 2017). We call this “R<sup>3</sup>” branching in reference to 3-dimensional Euclidian space—specifically, the volume of an organ.

In contrast, the metanephric kidney in mammals is an example of a less-common branching pattern where the tips of the tree of the ureteric bud (UB) are all located near the outer surface of the organ rather than filling the volume of an organ, as shown in Figure 1B. We term this “R<sup>2</sup>” branching in reference to 2-dimensional Euclidian space—specifically, the surface of an organ. This fundamental difference in branching pattern and organ organization has received little attention. Here, we attempt to understand the difference between R<sup>2</sup> and R<sup>3</sup> branching.

Why do most branching tree organs have an R<sup>3</sup> pattern, while the kidney has an R<sup>2</sup> branching pattern? In most cases, the tree serves to conduct liquid or gas between the exterior of the organ and epithelial cells located throughout the volume of the organ. For instance, in the mammalian lung, air moves bidirectionally through the branching tree between the

outside of the organism and the terminal branches of the airways that connect to alveoli where gas exchange occurs. Efficient respiration depends on the airway tree and alveoli having a near-maximal ratio of surface area to volume (Mauroy et al., 2004).

In contrast, the mammalian kidney has a more complex physiological function that is reflected in its organization (Little et al., 2016). The gross structure of the adult kidney is divided into two portions: the cortex, which occupies roughly the outer third of the kidney as measured radially; and the medulla, which occupies roughly the inner two-thirds. During development, the UB tips interact with cap mesenchymal cells to induce them to form secondary tubes, known as nephrons, that have an elaborate structure where a portion of the tube loops into the medulla and back out into the cortex; this looping into the medulla enables the metanephric kidney to raise the osmolarity of the urine that is important for terrestrial vertebrates. One end of the nephron tube connects to the UB, which becomes the collecting duct. The complex physiological function and



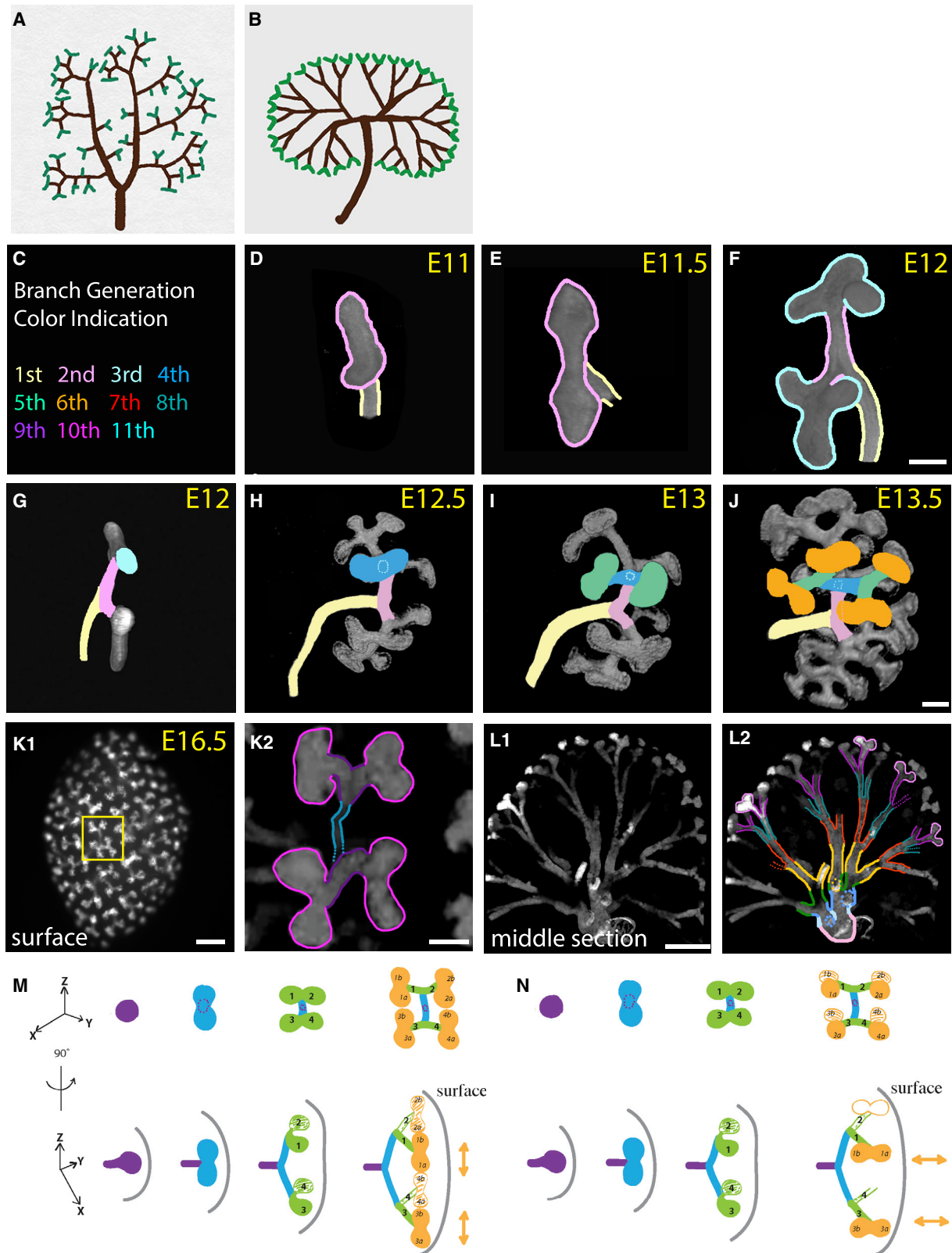


**Figure 1.  $R^3$  and  $R^2$  Branching Patterns**

(A and B) Comparison of  $R^3$  and  $R^2$  branching patterns. Highly schematized drawings of branching patterns of lung ( $R^3$ ) (A) and kidney ( $R^2$ ) (B) are shown. The drawings represent midplane sections through the developing organs. Brown color indicates major branches, while green color indicates terminal branches.

(legend continued on next page)

corresponding architecture of the kidney dictate that during the tips of the UB are all arranged near the surface of the developing kidney (Little et al., 2016), as shown in Figures 1K1 and 1L1.

The developmental  $R^3$  branching of the lung is largely stereotyped and uses three simple local modes of branching: domain branching, planar bifurcation, and orthogonal bifurcation (Metzger et al., 2008). Branching of the UB during mouse kidney development, the best-known  $R^2$  pattern, is largely stereotyped, as well (Short et al., 2018). Branching of the UB, which forms the collecting system of the kidney, consists almost entirely of one of the three patterns used in the lung, namely orthogonal bifurcation, though some steps are trifurcations.

At the molecular and cellular levels, much is known about mechanisms of forming a branch, but at higher levels of organization, the mechanisms patterning the branching tree remain unclear. Several models have been proposed to account for these branching patterns, including models based on a Turing reaction-diffusion mechanism (Lang et al., 2018) (Menshykau et al., 2019) or other physical processes (Hannezo et al., 2017; Short et al., 2018; Zubkov et al., 2015). As far as we know, no publication considers or even notes the difference between  $R^2$  and  $R^3$  branching patterns.

To get at the difference between  $R^2$  and  $R^3$  branching patterns, we re-examined UB branching. The tree of the UB in fetal mouse derives from the epithelial outgrowth of the Wolffian or mesonephric duct starting at embryonic day E10. The UB uses a simple pattern to form a tree that eventually consists of >1,000 terminal tips (Sampogna et al., 2015) (Short et al., 2013, 2014).

Figures 1D–1L2 shows UB branching during development; Figure 1C provides a color code of the number of each branching step. The initial bud (which we term “1st branch generation” and is equivalent to the term “root” used by Smyth’s group [Short et al., 2013]) that arises from the Wolffian duct (Figure 1E, yellow) first undergoes bifurcation and becomes a nearly T-shaped structure in which the secondary tip (second branch generation, relates to generation 1 in Smyth’s nomenclature) has an  $\sim 90^\circ$  angle to the parent segment that originally was the initial bud (Figure 1E, pink). Each tip at this stage gradually assumes a roughly triangular shape (Figure 1E, pink) and eventually forms a triple tip (third branch generation) (Figures 1F and 1G, light blue) that is in the same plane as the second branch generation.

Each of these six third branch generations undergoes bifurcation branching in which terminal tips (fourth branch generation) are orthogonal, i.e., at  $\sim 90^\circ$  angle (Figure 1G, dark blue), to their parent branches (third branch generation). The fourth branch generations then bifurcate again to form fifth branch generations that form at  $\sim 90^\circ$  angle to both the third and second branch generations (Figure 1I, green). This is an example of orthogonal bifurcation, as described in the lung (Metzger et al., 2008). Almost all UB branching beyond this step uses orthogonal bifurcation. All of this is compatible with previous reports (Sampogna et al., 2015; Short et al., 2013, 2014) and is provided here to set the stage for understanding the next step, which involves  $R^2$  versus  $R^3$  branching.

Importantly, starting with the sixth branch generation, orthogonal bifurcation in the kidney follows an altered but simple

pattern: the two newly formed child branch generations are perpendicular to their parent branch generation but parallel to their grandparent branch generation, as shown in Figure 1J (compare sixth orange to fifth green and fourth blue). Note in contrast that the fourth and fifth branch generations are perpendicular to both their parent and grandparent generations; this can be more easily appreciated in Figures 1I and 1H. This pattern continues repeatedly all the way to the completion of UB branching on postnatal day P3 (data not shown). In the kidney, the grandchild branch generations are always perpendicular to the parent and parallel to the grandparent generation. In contrast, for orthogonal bifurcation in lung the grandchild branches can be either parallel or perpendicular to the grandparent branch; often, especially after the initial round, apparently at random (see Figure S1 in Metzger et al., 2008). We term this relationship of the grandparent branches to the grandchild “Zu Sun” or 祖孙 orientation, meaning “grandparent-grandchild” orientation in Chinese. This relationship describes the dihedral angle formed between a branch, its parent, and its grandparent generation. Zu Sun orientation can be either parallel or perpendicular at each step, depending on the organ and situation. A schematic is shown in Figures 1M and 1N. Mouse kidney uses only Zu Sun orientation with parallel orientation (after the fifth branch generation), while lung uses both parallel and perpendicular orientations.

In the kidney, this repeated parallel Zu Sun orientation (i.e., the orange grandchild branches are parallel to the blue grandparent branch) in Figure 1M generates an  $R^2$  tree in which the final UB tips are all arranged at the peripheral surface

(C–L2) Branching morphogenesis of collecting ducts during fetal mouse kidney development: Reconstructed 3D data from collected Z stack images were analyzed from kidneys from E11 to P14. The order of branching segments is indicated by different colors as shown in (C).

(D–F) The ureteric bud (1<sup>st</sup> branch generation) bifurcates to form a T stage structure, the 2<sup>nd</sup> branch generation undergo shape change and then form triple tips. Kidneys were rotated  $90^\circ$  in Z direction to show a ventral view.

(G and H) 3<sup>rd</sup> branch generation bifurcate to form 4<sup>th</sup> branch generations. The child tips (4<sup>th</sup> branch generation) are perpendicular to both parents (3<sup>rd</sup> branch generation) and grandparent (2<sup>nd</sup> branch generation).

(I) 4<sup>th</sup> branch generation further bifurcate to generate two 5<sup>th</sup> branch generations that are perpendicular to parent (4<sup>th</sup> branch generation), but parallel to grandparent (3<sup>rd</sup> branch generation). Thus, 4 tips of 5<sup>th</sup> branch generations from same grandparent (3<sup>rd</sup> branch generation) form a “rosette” mode. This pattern, called orthogonal branching, is used repeatedly until the completion of branching morphogenesis by postnatal day 2 (J–L2).

Terminal tips are only seen at the peripheral surface (K1 and K2). No branch tips are observed in the interior volume at any stage (L1 and L2).

(K2) is enlarged from (K11).

Scale bars: 100  $\mu\text{m}$  in (D)–(F), (H), and (I). 200  $\mu\text{m}$  in (K1) and (L1). 50  $\mu\text{m}$  in (L2).

Data is based on manual examination of  $\geq 30$  kidneys from each of embryonic days (E) E11–17, and post-natal days (P) P0–4, P7, and P14. Representative images are presented.

(M and N) Schematics of two orthogonal branch patterns in mouse embryonic kidney and lung development. (M) shows the series of steps in kidney and lung orthogonal branching. (N) shows the steps that often occur in lung, but never in the kidney. Note the differences in the last step between these two organs and the surface views, respectively.

of the kidney (Figures 1K and 1L1). No tip is observed in the interior volume (Figure 1L1). In contrast, in the perpendicular Zu Sun orientation that is used for some rounds of orthogonal bifurcation in the lung (Figure 1N), the orange grandchild branches are perpendicular to the blue grandparent branch, resulting in some tips pointing away from the surface of the lung, contributing to the lung's  $R^3$  branching tree.

Note that as reported by others (Sampogna et al., 2015; Short et al., 2014) and as detailed in Table S1C: (i) during early kidney development, most branches form by bifurcation at right angles to their parent; (ii) later in development, the angles between sibling branches undergo a branch generation-specific reduction from the initial value of  $180^\circ$ ; (iii) branches change in length. These geometric features may have evolved to ensure proper final positioning of the branch termini.

### Computational Enumeration of Branching Patterns

To test whether the observed Zu Sun orientation pattern of the kidney—with every new branch from the sixth onward perpendicular to its parent and parallel to its grandparent branch—is somehow favorable to distributing tips on the surface, we need a way to predict how the tips will be spatially distributed if development were guided by alternative branching patterns. We do not have methods for creating altered branching patterns in live animals. Indeed, while there are many mutant mouse strains and at least two types of nutritional deficiencies that are known to have defects in kidney development, we did not find a report of a condition where the location of the tips of UB strictly at the surface of the kidney was perturbed (Hannezo et al., 2017; Sampogna et al., 2015; Short et al., 2014; Zhang et al., 2019; Yu et al., 2009; Lamberton et al., 2015; Menshykau et al., 2019; Rutledge et al., 2019). Even in the absence of *Wnt7b*, where the medulla does not form, the UB tips are still all arrayed at the outer surface of the embryonic mouse kidney (Yu et al., 2009). We therefore implemented a simple toy model for branching morphogenesis that abstracts away molecular and cellular details and focuses strictly on geometrical first principles. The toy model assumes that all branches will always be perpen-

dicular to their parents, and then explores every possible combination of dihedral angles (Zu Sun orientation) of branches relative to their grandparents by computationally generating virtual kidneys, following each possible branching pattern. Our toy model illustrates the spatial distribution of tube tips as dictated by explicit geometric rules but is silent about biologic processes.

We specify the branching pattern as a binary number, with each bit determining the Zu Sun branching direction (“perpendicular” or “parallel”) relative to the grandparent branch generation of a particular branch. These branching directions can be considered as defining a dihedral angle defined by the grandparent, parent, and daughter branch generations. Each binary sequence thus encodes a distinct pattern of branches, defined by the dihedral angles at each branching level. Figure 2A shows an example of how a branching tree is built up using the sequence 001111. This sequence describes events starting with the fourth branch generation. The first two branch generations (i.e., the initial first branch generation or root and the second branch generation, color coded yellow and pink in Figure 2A) cannot be described in terms of any earlier branches and instead serve to fix the coordinate frame of the model. Likewise, although the orientation of the third branch generation can be defined relative to the first branch generation, the orientation has no effect on the spatial distribution of endpoints and only serves to define the angle at which the root would emerge from the kidney. We therefore do not include the first, second, and third branch generations in our description string. We limited our search to a depth of six branching steps beyond these first three initial branches, for a total of nine branching levels, allowing us to describe a particular branching pattern as a six-digit binary number. To carry out the enumeration, we loop through every possible binary number; and for each number, we render the predicted branching pattern in three dimensions. Figure 2B shows several examples of different branching patterns produced by distinct binary sequences. In these simulations, branch lengths were deliberately chosen to make the branching pattern easily visualized in the plots.

To analyze the effect of branching pattern on the spatial distribution of tips, we iteratively generated all possible branching patterns for nine branching levels, setting all branch lengths equal as determined based on quantitative measurements from the E15 stage (Figure 3A). Then, for each branching pattern, we analyzed the distribution of end points to obtain numerical indicators of organ morphology. We evaluated endpoint distribution using several numerical metrics described below, with results summarized in Table S1B.

First, we calculated the distribution of distances from each endpoint to the centroid of all end points, which we take as the “center” of the kidney mass. The standard deviation of this distance distribution is a measure of the radial distribution of end points—if the end points were all located on a spherical surface, the standard deviation of distances from the centroid would be zero. The smaller the standard deviation, the closer the branching pattern is to distributing its end points at a fixed distance from the center. When we evaluated this figure of merit for all branching patterns (Table S1B, column 3), we found that the actual *in vivo* “Zu Sun” kidney branching pattern (defined by the binary string 001111) gave the lowest standard deviation of distances from endpoints to the centroid. One other branching pattern was tied for the lowest value, and all other branching patterns gave larger standard deviations. The motivation for measuring the standard deviation of distances is to ask whether the kidney branching pattern tends to place all the endpoints at a uniform distance from the centroid, which can be interpreted as saying that the distance distribution is highly concentrated into a narrow range of distances. On the other hand, standard deviation is derived from the Gaussian distribution and is only one way to quantify the narrowness of a distribution.

Another way to measure the broadness of the distance distribution—without relying on assuming a normal distribution—is entropy. If different end points have broadly varying distances from the center, the entropy of the distance distribution would be high, whereas if the endpoints are distributed at only a few distinct distances from the center, the entropy would be low. We therefore calculated

the entropy of the distance distribution (Table S1B, column 5) and found that the kidney branching pattern also gave the lowest entropy. That the *in vivo* kidney branching pattern was optimal in terms of standard deviation and entropy of the distribution of distances to the centroid suggests that this specific Zu Sun pattern may have evolved to produce a uniform placement of endpoints onto the surface of the kidney. However, we note that the kidney is not spherical, hence even if all end points were on the surface, their distances from the centroid would not all be identical. As an alternative figure of merit, we ask the degree to which the set of branch end points can approximate a two-dimensional surface. In principle, we could attempt to fit some specific surface, such as a sphere, to the point cloud and then take a residual distance. Again, we know the kidney is not spherical, and different branching patterns might give different best-fit shapes. In order to avoid assuming any particular form of the curved surface, we want a measure of closeness to a 2D surface that does not require any particular surface shape.

One way to do this is to calculate the fractal dimension, which is a numerical estimate of the dimensionality of the space spanned by a set of points. We estimate the fractal dimension using the correlation dimension estimate (Procaccia, 1983), a robust estimator of fractal dimension commonly used in analysis of dynamical systems. The results, given in Table S1B, column 6, show that the kidney branching pattern [001111] does not do particularly well in terms

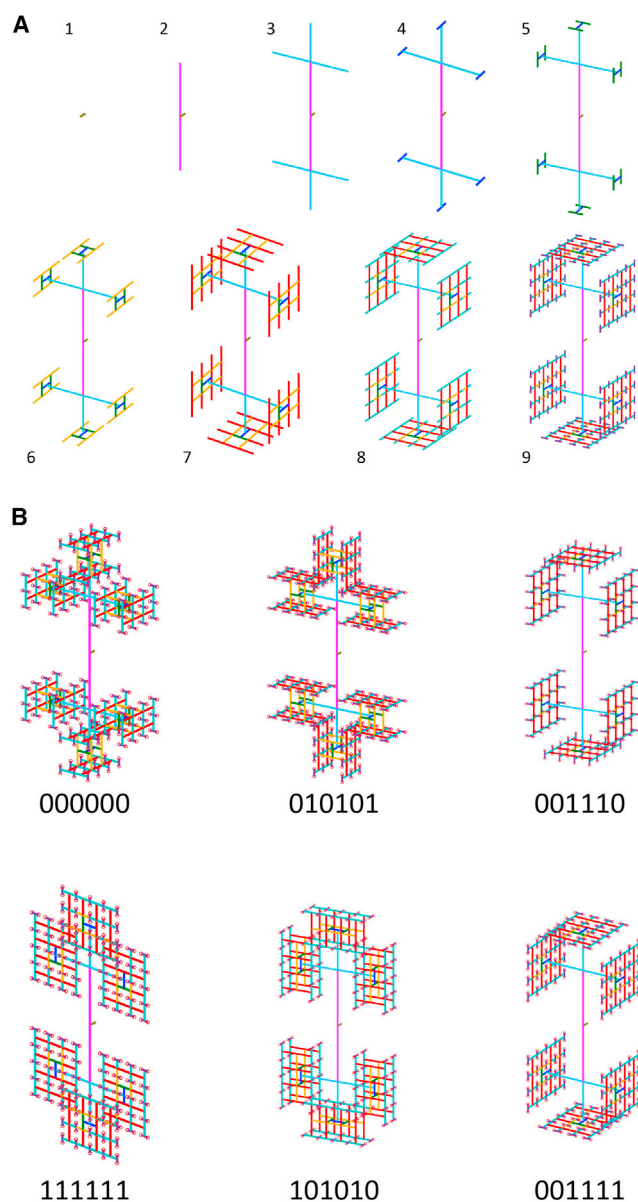


**Figure 2. Computational Enumeration of Branching Patterns**  
 (A) Steps in computational synthesis of a kidney branching pattern following the branching rule string [001111]. Successive branching levels, starting from the primary branch, are shown for nine branching levels as used throughout this paper. Colors of branches are chosen to match Figure 1C, except that the initial branch is indicated in gray rather than yellow in order to make it more visible. These branch patterns were generated using unequal lengths of branches chosen so as to make the different levels of branching more easily discerned.  
 (B) Different branching rule strings yield different spatial distributions of terminal points. Branching patterns generated by six of the 64 possible rule strings are illustrated. Sequences [000000] and [111111] are the extreme cases in which all branches are orthogonal or perpendicular to their grandparents, respectively. Sequences [010101] and [101010] are shown to illustrate the importance of the order of ones and zeros in the rule string. Sequence [001111] corresponds to the actual kidney *in vivo*, and the sequence above it, [001110] was shown to illustrate how even a single altered bit can yield a different endpoint distribution. These branch patterns were generated using the same branch lengths as in Figure 3.

of producing a fractal dimension close to 2. In fact, the kidney branching pattern stands out for giving the smallest fractal dimension. Only one other pattern [111111] gave a lower fractal dimension. However, we note that in all cases, the fractal dimension is closer to 2 than it is to 1, so the biological significance of these dimensionality estimates is unclear.

In addition to the distribution of endpoints in 3D space, we also considered whether different patterns might be optimal in terms of avoiding collisions between neighboring branches or end points. We calculated the fraction of end points whose nearest neighbor endpoint is closer than its sister endpoint, as a measure of the degree to which subtrees of the network might clash or overlap. All branching patterns tested showed a high fraction of endpoint clash by this criterion (Table S1B, column 7).

Finally, we considered steric clash of branches between all possible pairs of branches. Given  $n$  levels of branching, there are a total of  $(2^n - 1)(2^n - 2)/2$  unique pairs of branches that could clash, which for nine branching levels means that the number of potential steric clashes could be as high as 130,305. As seen in Table S1C, column 8, no steric clashes occurred for any branching pattern, which is the expected result given that branching remains entirely orthogonal at each stage.

### Influence of Branch Length and Angle Changes on Tip Distribution

The preceding results indicate that the Zu Sun branching pattern of the kidney is optimized for placing the termini on a single smooth surface

with minimal overlap between endpoints, which were the two main design goals we imagined the kidney would seek to satisfy during development. However, the model thus far assumed that each branch is strictly orthogonal to its parent.

This analysis ignored the observation that later in development, as a result of growth, the angles between sister branches are less than 180 degrees, as can be seen in Figure 1 and is tabulated for E15 in Table S1A. Might these angle changes, when combined with particular branching patterns, make some patterns more favorable than others? We modeled the angle change within our simulation by first generating the original branching pattern with branches orthogonal to their parents, and then changing the angles of all branches according to measured values at E15 as listed in Table S1A. (see Supplemental Information for methodological details). The effect of these angle changes is illustrated in Figure 2B. We applied the same angle changes to all branching patterns in our enumeration scheme, and then re-analyzed the endpoint distribution (results are listed in Table S1C). When branch lengths and angle changes are taken into account, the standard deviation of distances from end points to the centroid is second to lowest, and the entropy is the lowest, for the kidney branching pattern 001111 (Table S1C, columns 3 and 5). Thus, by these two criteria, the kidney branching pattern remains optimal in terms of endpoint distribution despite the dramatic changes in network geometry.

In terms of fractal dimension, when the length and angle changes were applied, we observed that the kidney branching pattern 001111 has the lowest fractal dimension for the set of end points compared to any other branching pattern (Table S1C, column 6). Interestingly, when we calculated the change in fractal dimension generated by the angle and branch length changes, by comparing results in Tables S1B and S1C, we found that the change was greatest for the

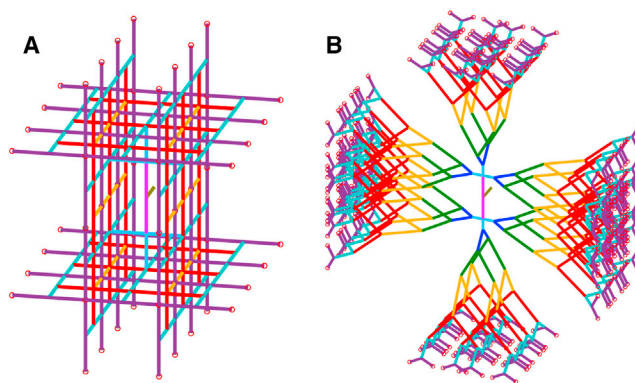


**Figure 3. Endpoint Distribution Determined by Kidney Branching Rules**

(A) Simulated branching pattern with rule sequence [001111] with all lengths set equal and all sister branches set at 180° apart from each other as seen in early stages of kidney development.

(B) Simulated branching pattern with rule sequence [001111] with branch lengths and angles specified according to measurements in actual kidneys at stage E15 as listed in Table S1A.

001111 branching pattern. This result suggests that the particular branching pattern seen during kidney development may have co-evolved with the geometrical changes (branch length and angle) so as to create an endpoint spatial distribution with a low fractal dimension, closer to 1 dimension than to 2.

We also asked how the angle change affected steric clash. Compared to the maximum number of potential steric clashes (calculated above to be 130,305 for nine levels of branching), the number of actual clashes was on the order of several thousand for all branching patterns. The *in vivo* kidney pattern 001111 did not stand out, although it was among the lower half of all patterns in terms of numbers of clashes. We speculate that the flexibility of branching tissues may mean that steric clash is not a serious problem that needed to be avoided in the evolution of a specific branching pattern.

### Final Thoughts

The function of an organ usually dictates its form; how an organ develops into its specific form is a foundational question in developmental biology. Here, we illustrate one approach to this question by enumerating all possible configurations of a branching network in which each daughter branch is orthogonal to its parent, as seen in the early development of the kidney, and then asking whether the actual branching pattern is favored in

terms of several figures of merit designed to evaluate the degree to which a given pattern results in endpoints distributed on a two-dimensional surface, as is the case with the branching tips in the kidney. We found that out of all possible branching patterns, the actual branching pattern used by the kidney *in vivo* was the most effective at placing endpoints in a single layer a uniform distance from the center of the organ, which is a key goal in kidney development. This result strongly suggests that a specific branching pattern was selected in evolution to achieve an organ-specific spatial arrangement. As we

enter the age of regeneration medicine, understanding the rules of UB branching may help us guide the regeneration of kidneys from stem cells (Boreström et al., 2018; Wu et al., 2018).

It is instructive to compare branching in the kidney to what is seen in other organs. Lung branching proceeds in two phases. Initially, the lung follows a complex pattern of branching from the sides of a tube, termed domain branching—which also contributes to space-filling in the lung—after which branching occurs primarily by two different sequences of bifurcation, both orthogonal bifurcation as in kidney, as well as a variant termed planar bifurcation. Although our current modeling framework does not allow us to represent the domain branching or planar bifurcation programs, we can directly represent the orthogonal bifurcation program of the lung, in which branches form orthogonal to their parent. Previous studies (Metzger et al., 2008) have found that this orthogonal bifurcation program in the lung consists of a mixture of dihedral angles, such that branches can form both orthogonal to and parallel to their grandparents. Our computational enumeration studies in Table S1B show that these two branching patterns, if one or the other is used exclusively, give dramatically different spatial distributions of endpoints, with [000000] and [111111] generating endpoint distribution fractal dimensions of 2.23 and 1.76, respectively. In fact, these

two branching patterns produce the maximum and minimum fractal dimensions seen among all rule sequences in [Table S1B](#), confirming the intuitive idea that all-perpendicular branching gives the highest dimensionality and all-parallel branching the lowest dimensionality. Given that the functional design of the lung requires endpoints (bronchi) to fill the three-dimensional interior of the lung, we would expect the all-orthogonal pattern to predominate, but in fact a mixture of orthogonal and parallel dihedral angles, with respect to grandparent branches, is observed in the orthogonal bifurcation pattern. It is thus interesting to consider whether the specific balance of patterns used in the lung is optimal in some sense beyond just space-filling.

We have considered here only two types of branching patterns. Undoubtedly others exist in nature; we hope that our discussion has at least provided a few tools to approach these alternative patterns.

#### SUPPLEMENTAL INFORMATION

Supplemental Information can be found online at <https://doi.org/10.1016/j.cels.2019.08.001>.

#### ACKNOWLEDGMENTS

WAL, KEM and WFM were supported by NSF grant DBI-1548297. KEM was supported by NIH NIDDK grants R01 DK074398, R01 DK091530 and P30 DK079307 (University of Pittsburgh O'Brien Kidney Center). RJM was supported by the UCSF Program for Breakthrough Biomedical Research, which is funded in part by the Sandler Foundation. We thank Evans Whitaker MD MLIS, UCSF Health Sciences Library and the California Digital Library for bibliographic support.

#### AUTHOR CONTRIBUTIONS

Conceptualization: RM, LM, WL, KM. Methodology: WY, WM, PB, RM. Software: WM. Validation: WY, WM, RM. Formal Analysis: WM, LM. Investigation: WY. Resources: WL, KM. Data Curation: WY. Writing Original Draft: WY, WM, KM. Writing – Review & Editing: WY, PB, RM, KM. Visualization:

WY, WM, LM. Supervision: KM. Project Administration: KM. Funding Acquisition: WL, KM

#### SUPPORTING CITATIONS

The following reference appears in the Supplemental Information: [Hama et al., 2011](#).

#### REFERENCES

Aristotle. (1961). *Parts of Animals* (Harvard University Press), p. 251.

Boreström, C., Jonebring, A., Guo, J., Palmgren, H., Cederblad, L., Forslöw, A., Svensson, A., Söderberg, M., Reznichenko, A., Nyström, J., et al. (2018). A CRISPR(e)R view on kidney organoids allows generation of an induced pluripotent stem cell-derived kidney model for drug discovery. *Kidney Int.* 94, 1099–1110.

Hama, H., Kurokawa, H., Kawano, H., Ando, R., Shimogori, T., Noda, H., Fukami, K., Sakaue-Sawano, A., and Miyawaki, A. (2011). Scale: a chemical approach for fluorescence imaging and reconstruction of transparent mouse brain. *Nat. Neurosci.* 14, 1481–1488.

Hannezo, E., Scheele, C.L.G.J., Moad, M., Drogo, N., Heer, R., Sampogna, R.V., van Rheenen, J., and Simons, B.D. (2017). A Unifying Theory of Branching Morphogenesis. *Cell* 171, 242–255.

Lamberton, T.O., Lefevre, J., Short, K.M., Smyth, I.M., and Hamilton, N.A. (2015). Comparing and distinguishing the structure of biological branching. *J. Theor. Biol.* 365, 226–237.

Lang, C., Conrad, L., and Michos, O. (2018). Mathematical Approaches of Branching Morphogenesis. *Front. Genet.* 9, 673.

Little, M.H., Combes, A.N., and Takasato, M. (2016). Understanding kidney morphogenesis to guide renal tissue regeneration. *Nat. Rev. Nephrol.* 12, 624–635.

Mauroy, B., Filoche, M., Weibel, E.R., and Sapoval, B. (2004). An optimal bronchial tree may be dangerous. *Nature* 427, 633–636.

Menshykau, D., Michos, O., Lang, C., Conrad, L., McMahon, A.P., and Iber, D. (2019). Image-based modeling of kidney branching morphogenesis reveals GDNF-RET based Turing-type mechanism and pattern-modulating WNT11 feedback. *Nat. Commun.* 10, 239.

Metzger, R.J., and Krasnow, M.A. (1999). Genetic control of branching morphogenesis. *Science* 284, 1635–1639.

Metzger, R.J., Klein, O.D., Martin, G.R., and Krasnow, M.A. (2008). The branching programme of mouse lung development. *Nature* 453, 745–750.

Procaccia, P.G.I. (1983). Characterization of Strange Attractors. *Phys. Rev. Lett.* 50, 346–349.

Rutledge, E.A., Parvez, R.K., Short, K.M., Smyth, I.M., and McMahon, A.P. (2019). Morphogenesis of the kidney and lung requires branch-tip directed activity of the Adamts18 metalloprotease. *Dev. Biol.* <https://doi.org/10.1016/j.ydbio.2019.06.012>.

Sampogna, R.V., Schneider, L., and Al-Awqati, Q. (2015). Developmental Programming of Branching Morphogenesis in the Kidney. *J. Am. Soc. Nephrol.* 26, 2414–2422.

Short, K., Hodson, M., and Smyth, I. (2013). Spatial mapping and quantification of developmental branching morphogenesis. *Development* 140, 471–478.

Short, K.M., Combes, A.N., Lefevre, J., Ju, A.L., Georgas, K.M., Lamberton, T., Cairncross, O., Rumballe, B.A., McMahon, A.P., Hamilton, N.A., et al. (2014). Global quantification of tissue dynamics in the developing mouse kidney. *Dev. Cell* 29, 188–202.

Short, K.M., Combes, A.N., Lisnyak, V., Lefevre, J.G., Jones, L.K., Little, M.H., Hamilton, N.A., and Smyth, I.M. (2018). Branching morphogenesis in the developing kidney is not impacted by nephron formation or integration. *eLife* 7, <https://doi.org/10.7554/eLife.38992>.

Walton, K.D., Freddo, A.M., Wang, S., and Gumucio, D.L. (2016). Generation of intestinal surface: an absorbing tale. *Development* 143, 2261–2272.

Wu, H., Uchimura, K., Donnelly, E.L., Kirita, Y., Morris, S.A., and Humphreys, B.D. (2018). Comparative Analysis and Refinement of Human PSC-Derived Kidney Organoid Differentiation with Single-Cell Transcriptomics. *Cell Stem Cell* 23, 869–881.

Yu, J., Carroll, T.J., Rajagopal, J., Kobayashi, A., Ren, Q., and McMahon, A.P. (2009). A Wnt7b-dependent pathway regulates the orientation of epithelial cell division and establishes the cortico-medullary axis of the mammalian kidney. *Development* 136, 161–171.

Zhang, H., Bagherie-Lachidan, M., Badouel, C., Enderle, L., Peidis, P., Bremner, R., Kuure, S., Jain, S., and McNeill, H. (2019). FAT4 Fine-Tunes Kidney Development by Regulating RET Signaling. *Dev. Cell* 48, 780–792.

Zubkov, V.S., Combes, A.N., Short, K.M., Lefevre, J., Hamilton, N.A., Smyth, I.M., Little, M.H., and Byrne, H.M. (2015). A spatially-averaged mathematical model of kidney branching morphogenesis. *J. Theor. Biol.* 379, 24–37.